Emissions of methane from coal thermal power plants and wetlands and its implications on atmospheric methane across the South Asian region

Mahalakshmi Venkata Dangeti[1], Mahesh Pathakoti*[1], Kanchana Lakshmi Asuri[1], Sujatha Peethani[2], Ibrahim Shaik[1], Rajan Sundara Krishnan[3], Vijay Kumar Sagar[4], Raja Pushapanathan[5], Yogesh Kumar Tiwari[4], and Prakash Chauhan[1]

[1]National Remote Sensing Centre (NRSC), Indian Space Research Organisation (ISRO), Hyderabad, India-500037
[2]Formerly at The International Center for Agricultural Research in the Dry Areas
[3]Lab for Spatial Informatics, International Institute of Information Technology (IIIT), Hyderabad-5000084, India
[4]Indian Institute of Tropical Meteorology (IITM), Pune, India-411008
[5]ICAR-Indian Institute of Soil and Water Conservation, Research Centre, Koraput, Odisha, India-763002
*Corresponding author: mahi952@gmail.com

Abstract. Atmospheric methane (CH_4) is a potent climate change agent responsible for a fraction of global warming. The present study investigated the spatio-temporal variability of atmospheric column-averaged (X) CH_4 concentrations using Greenhouse gases Observing SATellite (GOSAT) and TROPOspheric Monitoring Instrument onboard the Sentinel -5 Precursor (S5P/TROPOMI) data from 2009 to 2022 over the South Asia region. During the study period, the long-term trends in XCH_4 increased from 1700 ppb to 1950 ppb with an annual growth rate of 8.76 ppb year^{-1}. Among all natural and anthropogenic sources of CH_4, the rate of increase in XCH_4 was higher over the coal site at about 10.15±0.55 ppb year^{-1} (Paschim Bardhaman) followed by Mundra ultra mega power plant at about 9.72±0.41 ppb year^{-1}. Most of the wetlands exhibit an annual trend of XCH_4 more than 9.50 ppb year^{-1}, with a minimum rate of 8.72±0.3 ppb year^{-1} over Wular Lake. The WetCHARTs-based emissions of CH_4 from the wetlands were minimal during the winter and pre-monsoon seasons. Maximum CH_4 emissions were reported during the monsoon with a maximum value of 23.62±3.66 mg m^{-2} month^{-1} over the Sundarbans wetland. For the 15 Indian Agroclimatic zones, significant high emissions of CH_4 were observed over the Middle Gangetic Plains, Trans Gangetic Plains, Upper Gangetic Plains, East Coast Plains & Hills, Lower Gangetic Plains, and East Gangetic Plains. Further, the bottom-up anthropogenic CH_4 emissions data are mapped against the XCH_4 concentrations, and a high correlation was found in the Indo-Gangetic Plains region, indicating the hotspots of anthropogenic CH_4.

Keywords: GOSAT, S5P/TROPOMI, Column-averaged CH_4, South Asia, spatio-temporal, anthropogenic emissions.

1 Introduction

Atmospheric methane (CH_4) is one of the high-potential greenhouse gases (GHG) and plays a vital role in the chemistry of the atmosphere. In the troposphere, CH_4 oxidation is due to hydroxyl (OH) radical and produces carbon monoxide, carbon dioxide, and ozone in the presence of increased amounts of oxides of nitrogen. In contrast, in the stratosphere, oxidation of

CH_4 is by OH radical, atomic oxygen and chlorine (Nair and Kavitha, 2020). CH_4 has enormous potential for global warming, about 28 times that of CO_2 over 100 years (IPCC, 2021), and a comparatively short perturbation lifespan of about 12 years (Balcombe et al., 2018). Over the past decade, the research community has become more interested in anthropogenic CH_4 concentration due to its persistent rise in the atmosphere, and lack of knowledge regarding its source or sink (Huang et al., 2015). The long-term CH_4 observations from the National Oceanic and Atmospheric Administration (NOAA) have shown a yearly increase of 8 ppb year^{-1}, while Shadnagar, an Indian site, shows an increase of 10 ppb year^{-1} (Sreenivas et al., 2022). Though the emissions have increased over the past 20 years, the causes remain unclear. Recent research suggests that a combination of fossil fuel and agricultural emissions, with fluctuations in the CH_4 sink in the atmosphere, also plays a part (Schaefer et al., 2016; Worden et al., 2017; Turner et al., 2019; Zhang et al., 2022). The decadal budget indicates that relative uncertainties may range from 20 to 35 % for inventories of anthropogenic emissions in specific sectors (agriculture, waste, fossil fuels), 50% for emissions from burning biomass and emissions from natural wetland ecosystems, and 100% or more for emissions from other natural sources which include inland waters and geological sources (Saunois et al., 2024). Maasakkers et al. (2023) reported the annual gridded CH_4 emission inventory over the United States of America (USA) while meeting the US Environmental Protection Agency (USEPA) emission inventory standards at $0.1° × 0.1°$ spatial resolution. This data was submitted to the United Nationals in 2020, reporting improved uncertainties over the global Emission Database for Global Atmospheric Research (EDGAR) database. Geographically, India's wetlands comprise 4.7% of the nation's total land area (Bassi et al., 2014; Kavitha et al., 2016). The primary sources of CH_4 emissions include natural emissions from freshwater systems, wetlands, and geological sources; anthropogenic emissions come from waste management, agriculture, and the mining and burning of fossil fuels (Kirschke et al., 2013; Saunois et al., 2016a; Ganesan et al., 2019).

Wetlands are the natural sources that contribute 20 to 40% of global emissions and dominate the inter-annual variability (Parker et al., 2018). Only limited studies have been conducted in India about CH_4 discharge from wetlands. A recent study (Vinna et al., 2021) shows that natural wetlands could produce 50% to 80% more CH_4 emissions by 2100. According to Schlesinger et al. (2009), wetlands, rice paddies, and ruminants are the leading producers of CH_4 on the Indian sub-continent. According to Hayashida et al. (2013), there is a seasonal pattern in the CH_4 concentration over the Indian subcontinent, with higher values during the post-monsoon and minimum in pre-monsoon. Kavitha et al., (2016) used SCIAMACHY retrieved methane product over the Indian region to understand the spatio-temporal variations. The salient findings of this study are that during monsoon and post-monsoon, high XCH_4 values are observed in the Northern regions. Different seasonal behaviour is observed with seasonal peak in post-monsoon and low during monsoon in the Southern peninsular regions. These regional variations are due to the distribution of sources like livestock population, rice cultivation, wetland, biomass burning and oil and gas mining. Along with temperature, precipitation, and radiation, the CH_4 emissions from the natural wetlands might affect the region's heat budgeting, exacerbating global warming on a local, regional, and even global scale (Sakalli et al., 2017). Thermal power plants are responsible for a large amount of the GHG emissions from the energy sector. Each thermal power plant has a different set of emission factors for methane and nitrous oxide, based on operating conditions and combustion technology (Kang et al., 2019). The integrated measure of CH_4 includes contributions from the various vertical atmospheric layers, ranging from the Earth's surface measurement point to the uppermost layer of the atmosphere. Chandra et al. (2017)

studied the raised air mass in the 600–200 hPa height layer over northern India, which accounts for 40% of the seasonal CH_4 augmentation during the southwest monsoon season. Conversely, in the semi-arid region, the height over 600 hPa contributed up to approximately 88% of the amplitude of the XCH_4 seasonal cycle, while the atmosphere below 600 hPa contributed only around 12%. The feature of air mass transport processes in the Asian monsoon region is the main reason for the increased contributions from above 600 hPa across the northern Indian region.

Insufficient datasets exist regarding the CH_4 feedback originating from wetlands; a study on the precise estimation of CH_4 outflow from wetlands and its impact on local/regional global warming scenarios is urgently needed. The ability to identify spatial and temporal fluctuations in atmospheric CH_4 from space, due to recent technological developments in remote sensing, could help fill in the gaps left by measurements performed by ships, planes, and the ground (Frankenberg et al., 2008; Kuze et al., 2009; Kavitha et al., 2018). The present study focuses on the Implications of emissions from coal, thermal power plants, and wetlands on atmospheric methane over South Asia using XCH_4 data from Greenhouse gases Observing SATellite (GOSAT) and TROPOspheric Monitoring Instrument onboard the Sentinel-5 Precursor (S5P/TROPOMI) from 2009 to 2022. It has further analyzed the spatial and temporal pattern of atmospheric CH_4 variations and emissions and its correlation with anthropogenic CH_4 emissions from the bottom-up emission inventory of the EDGAR. The wetland methane emissions were addressed using WetCHARTs v1.31. over the top 10 wetland sites of the present study. The response of atmospheric CH_4 concentrations to anthropogenic emissions in various agroclimatic zones of India was further highlighted in this study using the XCH_4 data from 2001 to 2022.

2 Study Region

The distribution of CH_4 sources over the Indian region is shown in Figure 1. The focus of the study was three CH_4 source regions—coal fields, thermal power plants, and the Ramsar wetlands. More details about Ramsar wetlands can be found below. The number of coal mines in India varies from 1 to 65, and the top ten coal fields were selected for this study based on their production capacity. During 2019–2020, coal and lignite production ranged between 0.1 and 120.47 MT. The details of the studied coal mines are provided in Table 1. Similarly, Table 2 lists the thermal power stations according to their respective power generation.

The Ramsar Convention is an international agreement created in 1971 to protect wetlands and promote their sustainable use (https://rsis.ramsar.org). As of November 2022, the Ministry of Environment, Forests and Climate Change (MoEF&CC), Government of India, has identified 75 Ramsar Wetland sites in India, spanning a total area of 13,35,530 ha. Based on the total geographical area coverage (Table 3), the top 10 sites were selected for the current investigation. The size of these wetlands ranges from 423,000 ha (Sundarbans Wetland, West Bengal) to 18,900 ha (Wular Lake, Jammu and Kashmir) (https://indianwetlands.in/wetlands-overview/indias-wetlands-of-international-importance/; PIB Press Release on World Wetlands Day dated 26th August, 2022).
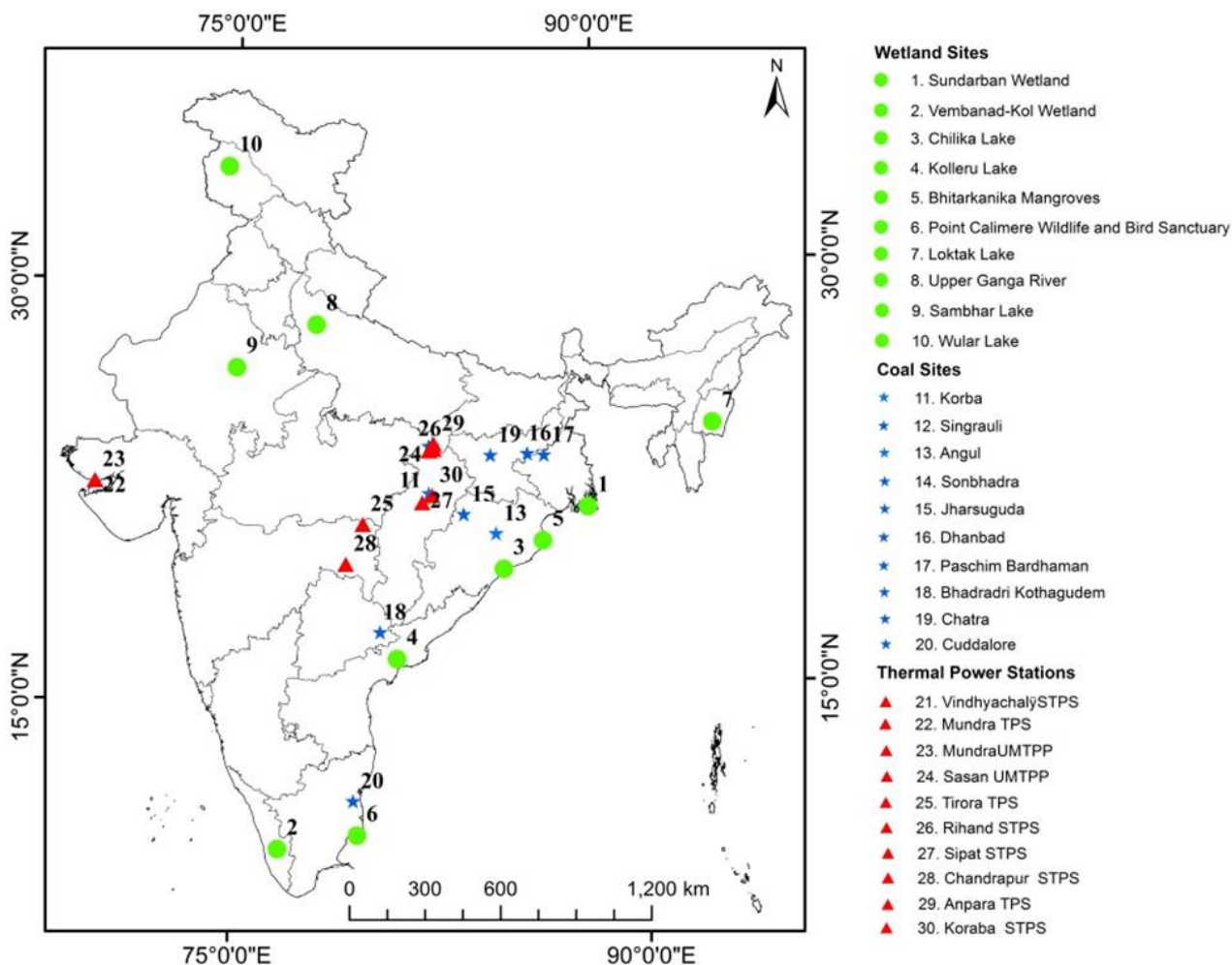
Figure 1. Study locations: a) top 10 coal mine locations in India based on production capacity indicated by star (★); b) top 10 thermal power stations denoted by triangle (▲); and c) top 10 wetlands selected based on the area represented by circle (●).

3 Data and Methodology

The GOSAT series developed by the Japan Aerospace Exploration Agency (JAXA) continuously monitors CO_2 and CH_4 from space (Kuze et al., 2009). The present study obtained the level 2 (L2) column CH_4 (XCH_4) from the GOSAT. Onboard the GOSAT, the Thermal and Near Infrared (NIR) Sensor for Carbon Observation Fourier-Transform Spectrometer (TANSO-FTS) is used to detect the CO_2 and CH_4 absorption spectra in the shortwave IR ($1.60\mu m$ & $2.0\mu m$) region (Kuze et al., 2009; Kavitha et al., 2018). Ground-based FTIR measurements of XCH_4 by the Total Carbon Column Observing Network (TCCON)

4

are used extensively to validate the GOSAT retrievals. Retrieval bias and precision of column abundance from GOSAT SWIR observations have been estimated as approximately 15-20 ppb and 1%, respectively (Morino et al., 2011; Yoshida et al., 2013). In the present study, the atmospheric CH_4 was obtained from 2009 to 2022 within a 100 km radius of the coal mines. The data

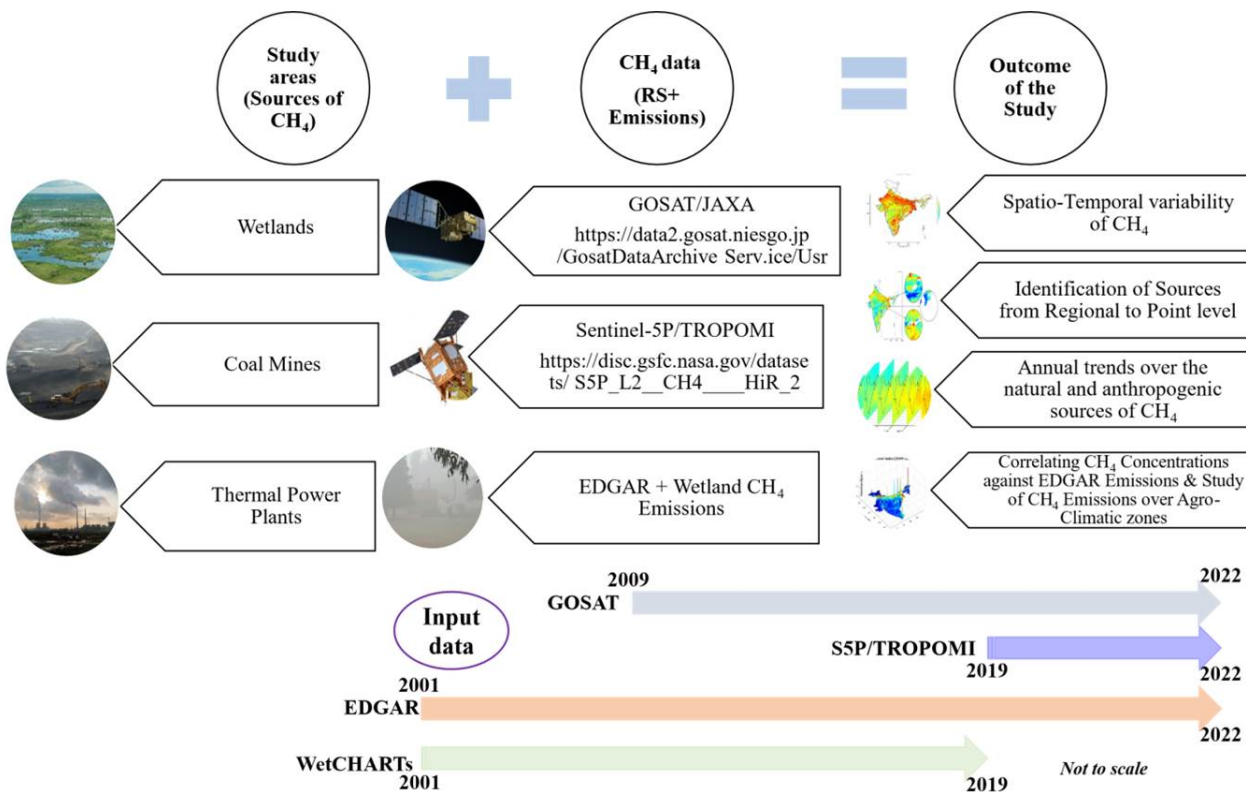95   corresponding to the quality flag (=0) was considered for the study only.

Figure 2. Data resources and study approach.

The Sentinel-5 Precursor satellite, launched on October 13, 2017, is equipped with the TROPOspheric Monitoring Instrument (TROPOMI), which tracks cloud characteristics, aerosols, and trace gases (Sentinel-5p, 2019). With a daily pass time of approximately 13:30 local solar time, the instrument's spectrometer measures reflected sunlight in the ultraviolet, visible, NIR, and SWIR spectral windows. The CH_4 retrieval algorithm uses the two spectral bands, i.e., reflectance in NIR (757-774

100   nm) and SWIR (2305-2385 nm) (Kozicka et al., 2023). Initially, retrievals based on TROPOMI had a spatial resolution of 7×7 km^2 (along-track × across-track, Lorente et al., 2021). From August 2019 to the present, the resolution has been increased to 5.5×7 km^2 (Sagar et al., 2022). The latest data version is now v2 from 2021-07-01 to the present. The quality flag (<0.5) was only considered as per the product readme file document (Sentinel-5p, 2019). Methane retrieval from TROPOMI agrees with ground-based FTIR XCH_4 retrievals from TCCON and the Network for Detection of Atmospheric Composition Change

105 (NDACC). The systematic differences of the bias-corrected XCH$_4$ data with respect to TCCON and NDACC data are, on average, -0.26±0.56% and 0.57±0.83%, respectively (Song et al., 2023).

The data within the coal mines and wetlands area were taken from 1 May 2018 to 30 April 2022. The individual shapefiles were given for each wetland field, and the satellite passes within the area were considered for the current study. As shown in Figure 2, a detailed procedure is explained in this section. The present study utilized the total anthropogenic emissions from
110 the EDGAR database (https://edgar.jrc.ec.europa.eu/gallery?release=v50&substance=CH4&sector=TOTALS, accessed on 1 November 2023). Uncertainties in the information on source intensity, activity, and other statistical data are key parameters for the uncertainties in the EDGAR emission inventory (Janardanan et al., 2017). Bottom-up inventory uncertainties range between 20% and 35% for agriculture, waste, and fossil fuel sectors; 50% for biomass burning and natural wetland emissions; and 100% or higher for natural sources such as geological seeps and inland waters for global methane emissions (Saunois et
115 al., 2024).

Further, the present study also utilized wetland methane emissions (mg m^{-2} month^{-1}) from WetCHARTs v1.3.1 (https://daac.ornl.gov/CMS/guides/MonthlyWetland_CH4_WetCHARTs.html) which is available at a spatial resolution of 0.5°×0.5° with monthly temporal resolution. The scale factor utilized here is 124.5 TgCH$_4$ yr^{-1}. We selected the coal fields based on production as shown in Table 1. The data on all coal mines in India, their production, and their location are available in Pai et
120 al. (2021) and Halder et al. (2024). Each district has open-cast or underground types of mines found in India, and the number of coal mines varies from 1 to 65. The coal/lignite production ranged from 0.1 to 120.47 MT during 2019-2020. The details of the coal mines in the present study are summarized in Table 1, and their locations are mapped in Figure 1.

Table 1. The district names, the total number of coal mines, total production, and their centroid (latitudes and longitudes) locations of mines in the respective districts.

S.No	District names	No. of Mines	Production (MT)	Latitude	Longitude
1	Korba	15	120.47	22.47	82.56
2	Singrauli	7	82.19	24.15	82.60
3	Angul	13	80.61	20.97	85.11
4	Sonbhadra	5	47.36	24.15	82.74
5	Jharsuguda	9	36.71	21.69	83.89
6	Dhanbad	51	31.25	23.76	86.46
7	Paschim Bardhaman	65	31.23	23.68	87.11
8	Bhadradri Kothagudem	14	30.16	17.57	80.58
9	Chatra	4	29.65	23.76	85.01
10	Cuddalore	3	23.46	11.55	79.50

The list is prepared based on the descending order of total production in each district in India. There are 262 thermal power stations with a full capacity of 229.335 Gigawatt (GW) and a total unit of 2689 in India, based on diesel, gas turbine, and steam as on March 31, 2020. Table 2 shows the list of thermal power stations.

Table 2. Top 10 thermal power plants based on their capacity.

S.No	Power Station Name	Installed Capacity (MW)	No. of Units	Latitude (N)	Longitude (E)
1	Vindhyachal STPS	4760	13	24.1	82.68
2	Mundra TPS	4620	9	22.82	69.55
3	Mundra UMTPP	4000	5	22.82	69.53
4	Sasan UMTPP	3960	6	23.98	82.62
5	Tirora TPS	3300	5	21.41	79.97
6	Rihand STPS	3000	6	24.03	82.79
7	Sipat STPS	2980	5	22.14	82.29
8	Chandrapur STPS	2920	7	20.00	79.3
9	Anpara TPS	2630	7	24.21	82.8
10	Korba STPS	2600	7	22.39	82.68

There are 11 new Ramsar sites identified in 2022 (total 75 sites) by the Ministry of Environment, Forests and Climate Change (MoEF&CC), India, covering a total area of 1,093,636 ha as of 2022. The present study considered the top 10 sites based on high area coverage (Table 3). The area ranges from 18,900 ha (Wular Lake) to 423,000 ha (Sundarban Wetland).

Table 3. Top 10 Wetland fields based on their area coverage.

S.No	Wetlands Location	Latitude (N)	Longitude (E)	Area (ha)
1	Sundarban Wetland	21.77	88.71	423000
2	Vembanad-Kol Wetland	9.83	76.75	151250
3	Chilika Lake	19.7	85.35	116500
4	Kolleru Lake	16.61	81.2	90100
5	Bhitarkanika Mangroves	20.65	86.9	65000
6	Point Calimere Wildlife Sanctuary	10.31	79.63	38500
7	Loktak Lake	24.43	93.81	26600
8	Upper Ganga River	28.55	78.2	26590
9	Sambhar Lake	27	75	24000
10	Wular Lake	34.26	74.55	18900

4 Results and Discussion

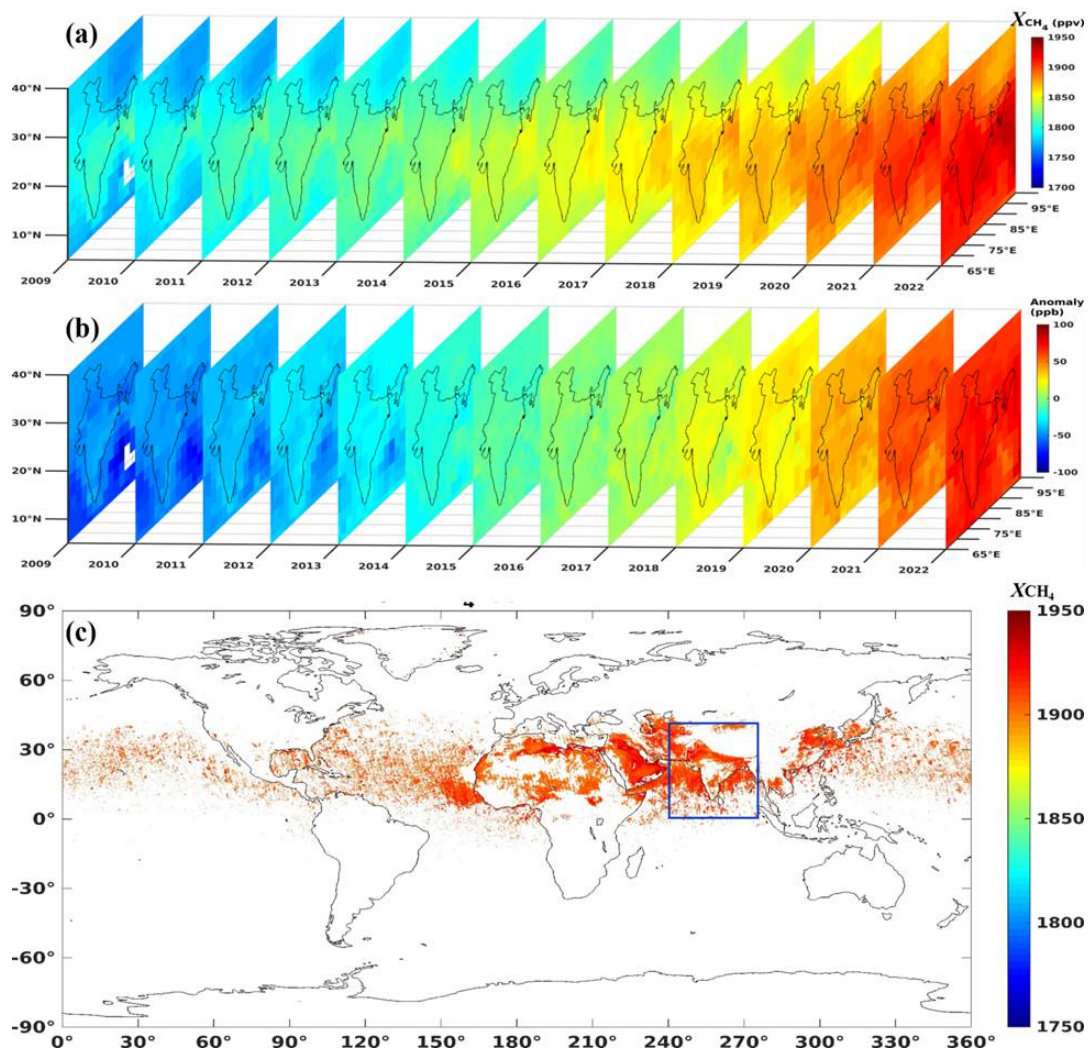## 4.1 Spatio-temporal variability of Space-based Atmospheric CH$_4$

Figure 3. a) Remote Sensing (GOSAT) of atmospheric CH$_4$ variability over the Indian sub-continent; b) Anomaly during 2009 to 2022; and c) identification of probable high CH$_4$ concentration using S5P/TROPOMI data from 2019 to 2022 over the study region.

In the present study, we examined the annual space-time distribution of the XCH$_4$, obtained from the GOSAT-1 and GOSAT-2 over South Asia as shown in Figures 3a-b from 2009 to 2022 (N=14 years)—the long-term trends in XCH$_4$ increased from 1700 ppb to 1950 ppb from 2009 to 2022 with an annual growth rate of 8.76 ppb year^{-1}. This growth rate is statistically tested with a p-value less than 0.05 for n=3803 observations. A distinct, evident annual growth in CH$_4$ is seen over the Indian

subcontinent. Figure 3b shows the spatio-temporal residuals calculated using the data from 2009 to 2022. Residuals indicate
that the acceleration of CH_4 emissions in India has been significant since 2015. Before 2015, the CH_4 concentrations were
lower by 20 ppb to 50 ppb compared to the total mean of the study period, indicating a slow rise in CH_4 activities. However,
post-2015, an increase of CH_4 was observed at a maximum of 100 ppb compared to the total mean, which indicates the surged
emission rates from varied sources of CH_4 (Lu et al., 2023). To identify the critical potential high emission zones of CH_4,
the present study applied the 90th percentile statistical filter, as shown in Figure 3c. The percentile is often used to detect the
points that are significantly different from the rest of the data. Statistically significant high concentrations of CH_4 are observed
in tropical regions (Feng et al., 2023). In the blue highlighted box (Latitude: 0°–40°N and Longitude: 60°–100°E), higher
concentrations of CH_4 were observed in the Indo-Gangetic Plain (IGP) and northwest (NW) areas of India, southeast of China,
and NW of China. Southern China and north China are marked with wetlands and rice paddy fields, which are the primary
sources of CH_4 (Kavitha et al., 2018; Chandra et al., 2019; Guo et al., 2023). High concentrations of CH_4 over the IGP and NW
of India are due to the population density and various industries that contribute to the emissions of CH_4 and emissions from
the rice paddy fields, respectively. In the present study, Figure 1 also shows the locations of coal and thermal power plants in
India. Globally, the tropical wetlands ecosystem accounts for about 20% of the total global source (Saunois et al., 2020; Shaw
et al., 2022), evidenced by bottom-up and top-down inventories. The study in the following sections assessed the CH_4 growth
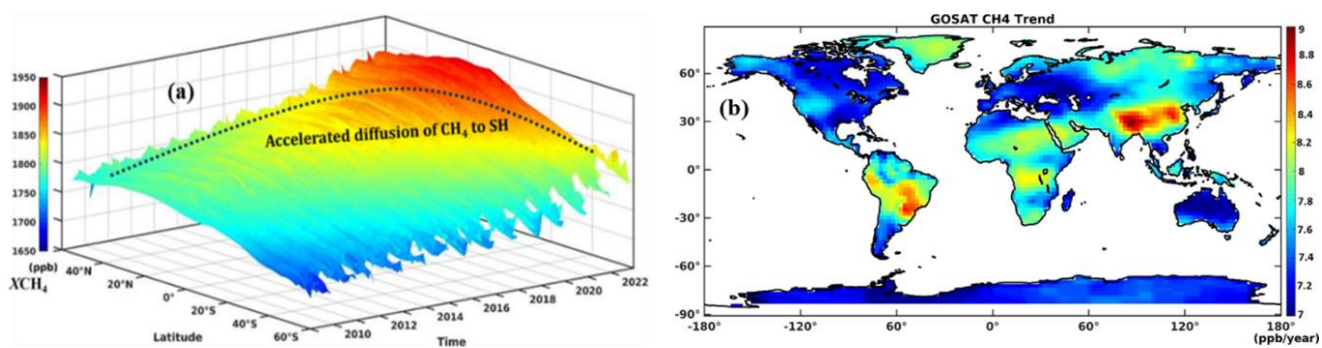rate associated with the source type over the Indian region.

Figure 4. (a) Spatiotemporal distribution of annual XCH_4 as a function of latitude during 2010 to 2022. (b) Global XCH_4 trend (ppb
year^{-1}) using GOSAT data.

Figure 4 shows the spatiotemporal distribution of XCH_4 as a function of latitude, which depicts the annual variability at each
latitude covering the northern and southern hemispheres (SH). There is a transparent latitudinal gradient in space. A strong
diffusion of CH_4 is observed from the northern hemisphere to SH during 2009 to 2022. During 2010, the XCH_4 was distributed
nearly constantly at all latitudes, indicating the stability of emissions from natural and anthropogenic sources. However, the
gradient between the NH and SH has narrowed down with a growth rate of 12 ppb year^{-1} in 2022, reflecting the dominance
of anthropogenic emissions over the tropics and unidentified leaks from the tropical wetlands and natural gas (Rocher-Ros et
al., 2023). More thoroughly, the characteristics of regional and global spatiotemporal variations are revealed by the continuous

XCH$_4$ data in space and time. As shown in Figure 4, it displays a latitudinal gradient, and each latitudinal zone's growth tendencies are comparable. Figure 4b shows XCH$_4$ has increased the global mean trend from 7 ppb year^{-1} to 9 ppb year^{-1}. There are hotspots in the XCH$_4$ trend observed in the Tibetan plateau (8.2 to 9 ppb year^{-1}), South America (8.2 to 8.8 ppb year^{-1}), and the African continent (8 to 8.4 ppb year^{-1}), and in the rest of the world varies from 6.75 to 8 ppb year^{-1}. Similarly high values were reported in the Tibetan plateau from 2010 to 2022 (Wei et al., 2019) and 8 ppb year^{-1} (Song et al., 2023) from 2009 to 2021 using GOSAT data.

4.2 Assessment of XCH$_4$ over different source types in India

Figures 5a-c show the monthly time series of XCH$_4$ over the specific sources of CH$_4$ plotted in the Indian region from 2009 to 2022. Over the Indian sub-continent and south-east Asia, October to November exhibits the highest amounts of CH$_4$, while March through June often sees the lowest (Sreenivas et al., 2016; Song et al., 2023), because of the enormous diversity in the climate zones of the Asian region. The seasonal cycle (peak and trough) of XCH$_4$ is strongly associated with the vegetation during the active phase of cultivation and reduced photochemical reaction by the hydroxyl radicals, respectively. The major sink for CH$_4$ is by the oxidation of OH radical in the troposphere which removes 90% of CH$_4$ from the atmosphere (Crutzen et al., 1991). However, the potential available of OH radical in the atmosphere is not steady and changes rapidly depending upon the presence of solar ultraviolet radiation and other trace gases such as ozone, oxides of nitrogen (NO+NO$_2$), and water vapor (Sreenivas et al., 2016).

Over the coal, thermal, and wetlands, the XCH$_4$ shows typical seasonal behavior, with maximum activity during the post-monsoon (October-November) and minimum activity in the pre-monsoon (March-May), as shown in Figure 6. A seasonal maximum of XCH$_4$ was observed over coal and thermal power plants from September to October and a minimum in pre-monsoon (March to May). In the case of wetlands, a shift in seasonal maxima varies from site to site, indicating their respective active phase of methanogens and the magnitude of the seasonal amplitude, which runs as a function of the individual wetland area. Methanogens are microscopic organisms that break down organic substances in an oxygen-free environment. Thus, wetlands are perfect for methanogens to grow and release CH$_4$ since they are usually oxygen-poor, moist habitats (Zhang et al., 2023). Therefore, the present study investigated the above-listed wetlands. Most of the wetlands exhibit an annual growth rate of XCH$_4$ greater than 9.50 ppb year^{-1} with high concentrations over Sundarbans wetland (Area = 423000 ha) with pronounced seasonality at all sites and lower concentrations over Wular Lake (area = 18900 ha) with an annual trend of 8.72±0.3 ppb year^{-1}. During the examination period, the seasonal trends (slope) at each location, as summarised in Tables 1-3, were evaluated using Sen's slope-based Mann-Kendall test with a significance of p-value < 0.05 (Pathakoti et al., 2021). The rate of increase in XCH$_4$ was higher over the Upper Ganga (area = 26590 ha) with a slope of 9.82±0.52 ppb year^{-1} and followed by Vembanad-Kol Wetland (area = 151250 ha) with a slope of 9.69±0.44 ppb year^{-1}. Over the Sundarbans wetlands, West Bengal (area= 423000 ha) the rate of increase in XCH$_4$ is 9.54±0.51 ppb year^{-1}. To investigate further, the present study quantified the source-based natural CH$_4$ fluxes from each wetland using the WetCHARTs data in the following section.

Typically, the Indian climate is hot and humid, causing disturbances in the rainfall patterns; an increase in the waterlogged soils expands the wetlands (Zhang et al., 2023). Typical tropical wetlands are acting as positive feedback to climate change
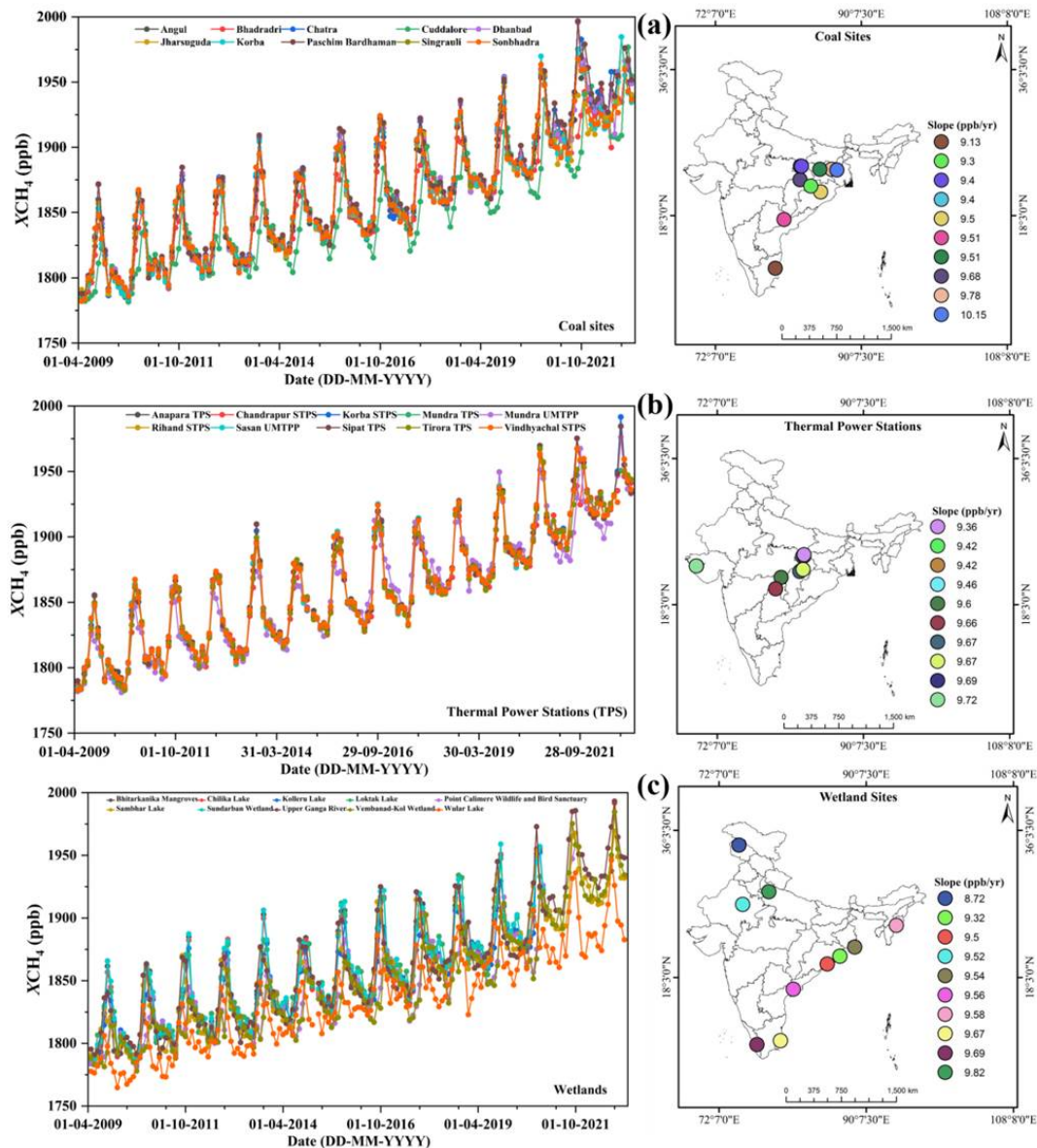
Figure 5. Monthly time series of XCH$_4$ over the a) wetlands, b) thermal power stations, and c) coal fields: sources of emissions, along with the overall growth rate at the respective site.

(Salimi et al., 2021). Irrespective of the power production capacity, over the thermal power plants, the CH$_4$ exhibited stabilized seasonality at each location. However, the growth rate of XCH$_4$ was higher over the Mundra Ultra Mega power plant (UMPP), Gujarat with a slope of 9.72±0.41 ppb year^{-1} followed by Mundra Thermal power station with a slope of 9.69±0.4 ppb year^{-1}.

195   The Mundra TPS and UMPP, Gujarat have a total power capacity of 8620MW with 14 units. With 2630 MW installed power
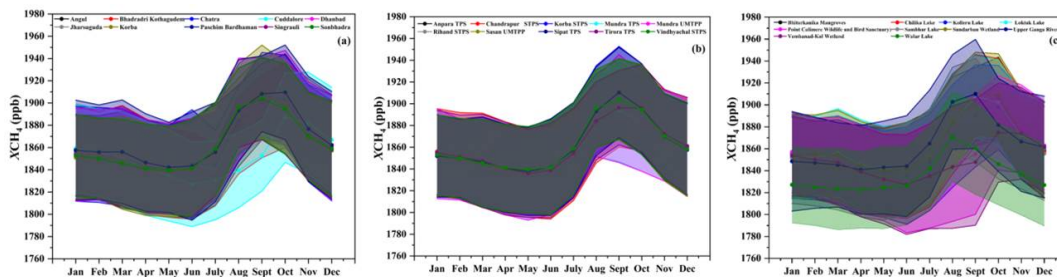
Figure 6. Seasonal XCH_4 over a) coal fields, b) thermal power stations, and c) wetlands.

capacity the Anpara TPS exhibited an XCH_4 growth rate of 9.36±0.5 ppb year^{-1}. This indicated the higher potential power plants contribute more CH_4 emissions into the atmosphere. Over the coal mines, Paschim Bardhman (31.23 MT, 65mines) shows a high XCH_4 trend of about 10.15±0.55 ppb year^{-1} followed by Dhanbad (31.25 MT, 51mines), Korba (120.47 MT, 15mines) which shows XCH_4 trend of 9.78±0.53 ppb year^{-1} and 9.68±0.52 ppb year^{-1}, respectively. Angul (80.61MT, 13 mines) and Chatra (29.65 MT, 4 mines) show XCH_4 trend of 9.51±0.5 ppb year^{-1}. The lowest annual trend in XCH_4 was observed over the Cuddalore coal mine (23.46 MT, 3 mines) which is about 9.13±0.4 ppb year^{-1}. Anthropogenic emissions influence the methane growth trend. Wetland and biomass burning emissions determine the interannual variability (Fo et al., 2024).
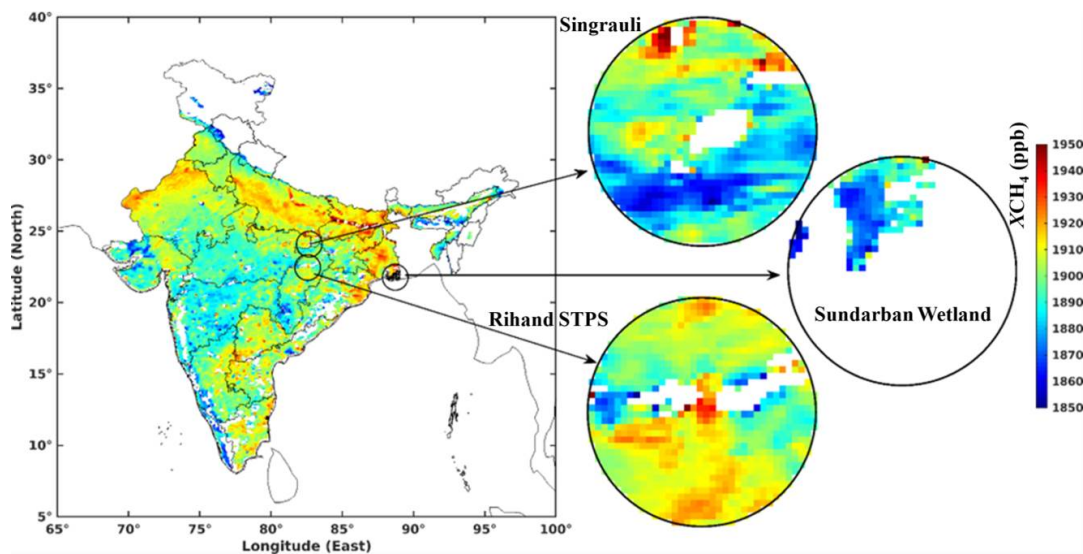
Figure 7. S5P/TROPOMI XCH_4 gridded to $0.05° \times 0.05°$ over the Indian region and XCH_4 over wetland, coal, and thermal power plant sites with a radius of 100 km.

Figure 7 shows the continuous XCH_4 data from the S5P/TROPOMI at $0.05° \times 0.05°$, complementing the GOSAT efforts in monitoring the XCH_4 dynamics in space and time. We demonstrated the spatiotemporal variation characteristics of XCH_4 more

comprehensively at three different source type locations (wetland, coal, and thermal power plant). High XCH_4 concentrations over the coal and thermal power station sites, and relatively lower concentrations in the wetland site. We concluded that the high-resolution S5P/TROPOMI has the potential to detect the point source variability. The growth rates of XCH_4 over the wetlands compete with coal sites, indicating an equivalent anthropogenic source. Results of the analysis in the context of thermal power plants and coal mines indicate that the emissions from the fossil fuel industries are significant, and the release of CH_4 into the atmosphere is commensurate with the production of the power and mining capacity.

4.3 CH$_4$ emission from India's wetlands

In addition to the anthropogenic emissions, the present study utilised the global monthly wetlands emission estimates from the Wetland Methane Emissions and Uncertainty (WetCHARTs v1.3.1) inventory (Bloom et al., 2017a, b; Bloom et al., 2021). The figure 8a shows the monthly CH_4 emission over India's top 10 wetland sites from 2001 to 2019 and figure 8b represents the long-term seasonally averaged CH_4 emission over wetlands. Emissions of CH_4 from the wetlands were minimal in the winter season (December to February) and pre-monsoon (March to May). In the tropical region, winter and pre-monsoon seasons are considered dry months with moderate to high temperatures and less precipitation.
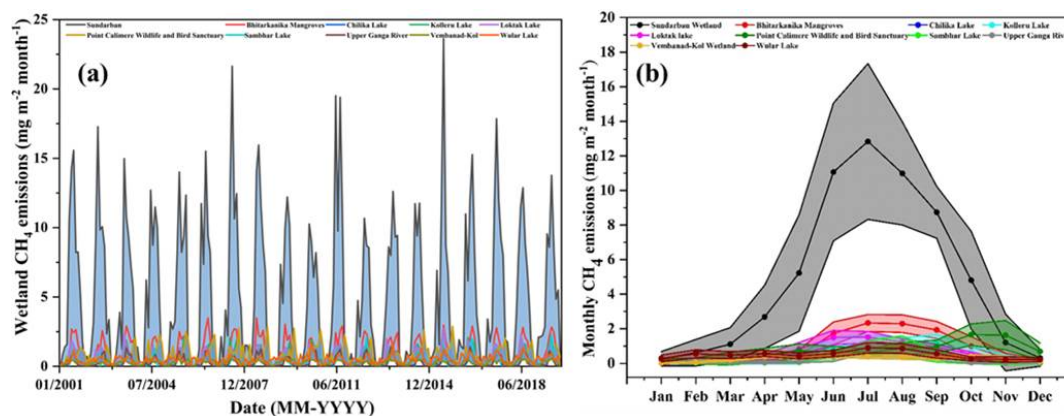
Figure 8. (a) Monthly Time series of Methane emissions (mg m^{-2} month^{-1}) over the wetland sites, (b) Seasonal methane emissions over the wetland sites from 2001 to 2019.

A study by Peng et al. (2022) and Feng et al. (2022) hypothesized that warmer and wetter wetlands contribute significantly to the high CH_4 emissions to the atmosphere. Typical climatological (1991-2020) mean temperature (accumulated seasonal precipitation) over India during winter, pre-monsoon, monsoon, and post-monsoon are 20 °C (23 mm), 28 °C (98 mm), 26 °C (867 mm) and 23 °C (106 mm) respectively (https://climateknowledgeportal.worldbank.org/country/india/climate-data-historical). At all the wetland study sites during the study period, the maximum CH_4 emission was reported during the monsoon months with a maximum value of 23.62$\pm$3.66 mg m^{-2} month^{-1} over the Sundarbans wetland, which is the largest protected wetland of India and mangrove forest in the world. Besides climatic conditions, the emissions of CH_4 are positively correlated

13

with the size of the wetland, thus reporting maximum CH_4 emission over the Sundarbans site. High natural CH_4 emissions during the monsoon positively correlate with the atmospheric XCH_4 concentrations.

Further, Mann-Kendall-based statistical analysis was carried out to assess the annual trend in the CH_4 emissions and found significant trend over the Wular Lake, with an increasing rate of 0.04 mg m^{-2} year^{-1} with a p-value of 0.01. An annual trend of XCH_4 was over this study is about 8.72$\pm$0.3 ppb year^{-1}. The current research highlights the need for further investigation to correlate in detail the temperature and associated precipitation influence on methane oxidation and microbial activities, thus modulating the CH_4 emissions from the wetlands.

4.4 Long term seasonal winds over the source locations
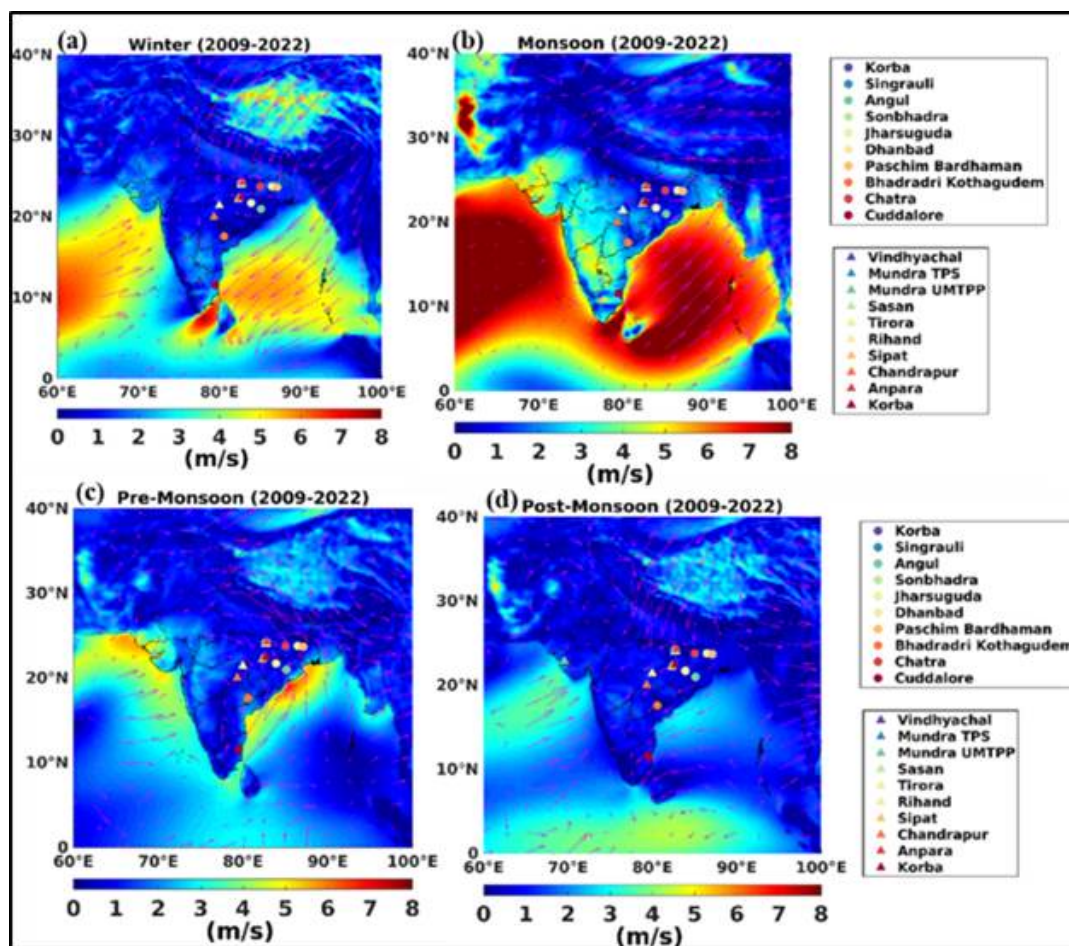
Figure 9. Long-term seasonal winds for source types (coal and thermal power plants) for the period 2009-2022: (a) winter, (b) monsoon, (c) pre-monsoon, and (d) post-monsoon respectively.

The 10 m u wind component of wind from ERA5 which is reanalysis product is used in the present study for the period 2009-

235 2022. The Figure 9 shows the long-term seasonal winds for coal and thermal power plants for the period 2009-2022. During winter, winds are primarily from northeast (NE) direction with low wind speeds at the study locations. During monsoon and pre-monsoon majority of winds are from southwest (SW) direction with medium to high wind speeds arriving at the source locations. At the coal and thermal power plants, winds from the SW during the pre-monsoon, which transports relatively clean airmass from the ocean to land, could also influence the observed low CH_4 concentrations along with the continued source

240 activity and seasonality. Quantification of CH_4 fluxes with an improved accuracy also needs required information about the prevailing winds at the source locations. Bussmann et al. (2024) established a detailed relationship between modulation in CH_4 fluxes against the wind speed and direction in his studies.
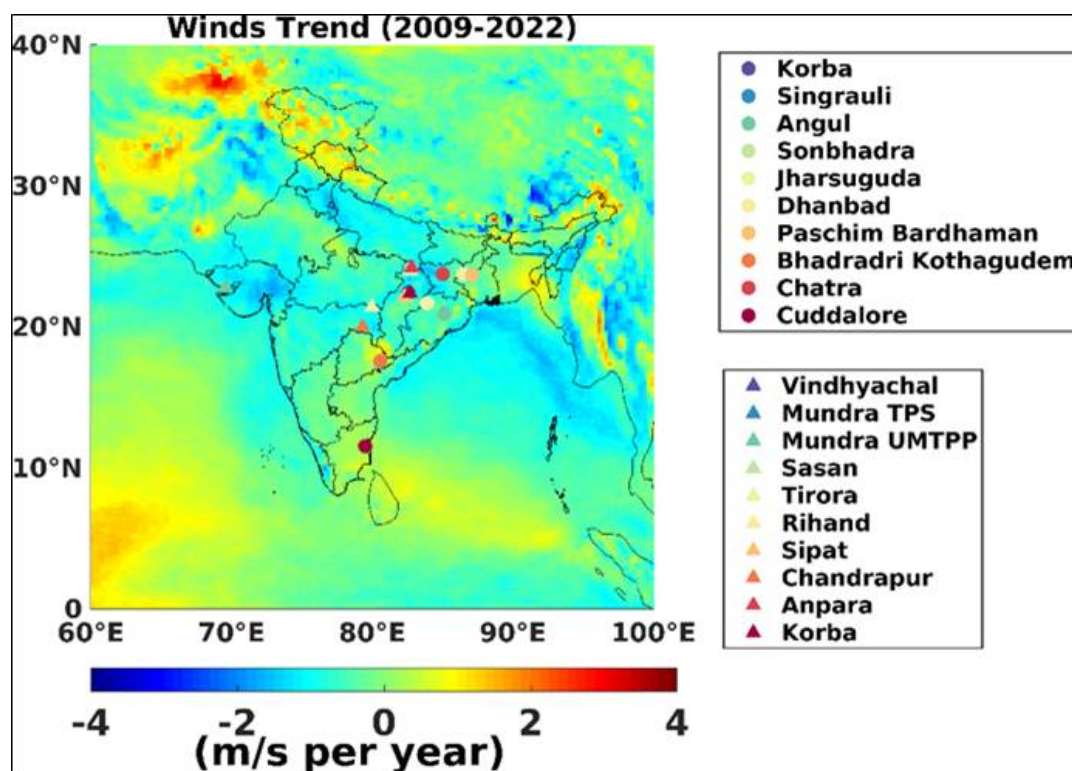
Figure 10. Long-term spatial trend of winds over the Indian region covering source types (coal and thermal power plants) for the period 2009-2022.

Figure 10 shows the trend in wind speeds over the coal and thermal power plants from 2009-2022. Around the coal mine sites, a positive trend in wind speed is observed over the Cuddalore coal mine site (0.42 ms^{-1} year^{-1}), whereas the remaining

245 coal mine sites show a negative trend in wind speed. The maximum negative trend is observed over the Sonbhadra coal mine site (1.21 ms^{-1} year^{-1}), and the minimum negative trend is observed over the Bhadradri Kothagudem coal mine (0.18 ms^{-1} year^{-1}). A negative trend in wind speed is observed over all the thermal power plants, with a maximum trend observed over

15

the Vindhyachal STPS (1.23 ms^{-1} year^{-1}) and a minimum over the Sipat STPS (0.63 ms^{-1} year^{-1}). Over the wetland sites, a positive trend in wind speed is observed over the Point Calimere Wildlife and Bird Sanctuary (0.25 ms^{-1} year^{-1}) and Wular

250 Lake (0.20 ms^{-1} year^{-1}). All the remaining wetland sites show a negative trend in wind speed. Besides the surface emissions, column CH$_4$ values are also varied by the background flow advection and unstable boundary layer due to strong convection (vertical mixing) in the daytime (Ricaud et al., 2014; Francis et al., 2023). A negative trend is observed over the source locations in the present study, indicating relatively slower dispersion at these locations, thus modulating column CH$_4$ values.

4.5 CH$_4$ emissions over India's Agroclimatic zones
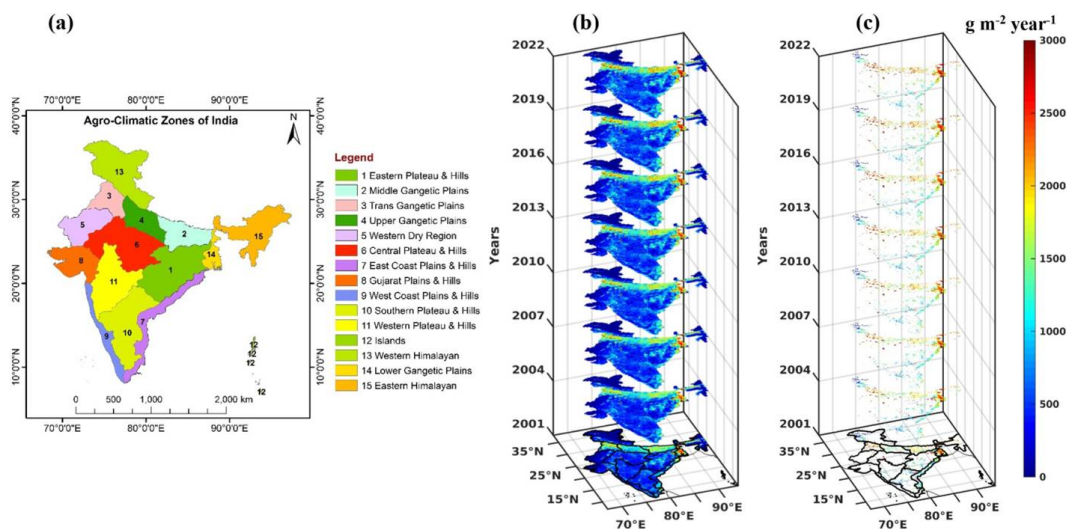
Figure 11. a) Agroclimatic zones of India, b) bottom-up CH$_4$ emissions inventory of EDGAR, and c) 90th percentile statistical filter applied on CH$_4$ emissions from 2001 to 2022.

255 India is divided into 15 agroclimatic zones according to the combination of soil types and climatic conditions (Choudhary and Sirohi, 2022). These zones offer a structure for the nation's development and execution of agricultural policies and practices. The crops and farming methods that are most appropriate for the environmental conditions in each zone are distinct from one another. Out of natural and anthropogenic sources of CH$_4$, agricultural activity is also one of the dominant contributors to CH$_4$ dynamics in the atmosphere. Figures 11a-c show India's 15 agroclimatic zones and spatiotemporal trends of CH$_4$

260 emissions obtained from the bottom-up emission inventory of EDGAR (Crippa et al., 2020) from 2001 to 2022. Significant high emissions of CH$_4$, as shown in Figure 11c, were reported over the Middle Gangetic Plains-MGP (2), Trans Gangetic Plains-TGP (3), Upper Gangetic Plains-UGP (4), East Coast Plains & Hills-ECPH (7), Lower Gangetic Plains-LGP (14) and East Gangetic Plains-EGP (15). These agroclimatic zones have active farming in rice, wheat, sugarcane, maize, millet, gram, cotton, etc. Besides traditional farming, the Lower Gangetic Plains has also actively contributed to livestock, horticulture,

265 and forage production (Ahmad et al., 2017). Among all 15 agroclimatic zones, the MGP, TGP, UGP, ECPH, LGP and EGP

have exhibited high emissions of CH$_4$ indicating the diversification of agricultural practices and homogenous traditions of agricultural production. Rice- wheat (R-W) based production system is mainly being practiced in this region which is causing negative effects on climate (Taneja et al., 2019). CH$_4$ emissions over the Northwest region are exhibiting weak contribution compared to other agroclimatic zones of India.

270 **4.6   Spatial correlation between XCH$_4$ concentrations and emissions over India**

To understand the relationship between India's high XCH$_4$ concentration zones against emissions, we have computed pixel-level correlation between S5P/TROPOMI measured XCH$_4$ concentrations and bottom-up inventory of EDGAR-based XCH$_4$ anthropogenic emissions. Figures 12a-c shows XCH$_4$ concentrations from S5P/TROPOMI, EDGAR-based anthropogenic emissions, and their correlation coefficient. The spatial patterns of XCH$_4$ concentrations agree well with the high-emission
275 regions. The correlation coefficient 'r' is strongly positive on in the IGP region, shows that more CH$_4$ emission into the atmosphere through rapid industrial activity and anthropogenic contribution from human activity due to high population density. Besides the IGP region, the 'r' value is also strong in the east and northeast region due to the emissions from natural sources such as agricultural activities, livestock, and wetlands (Behera et al., 2022).
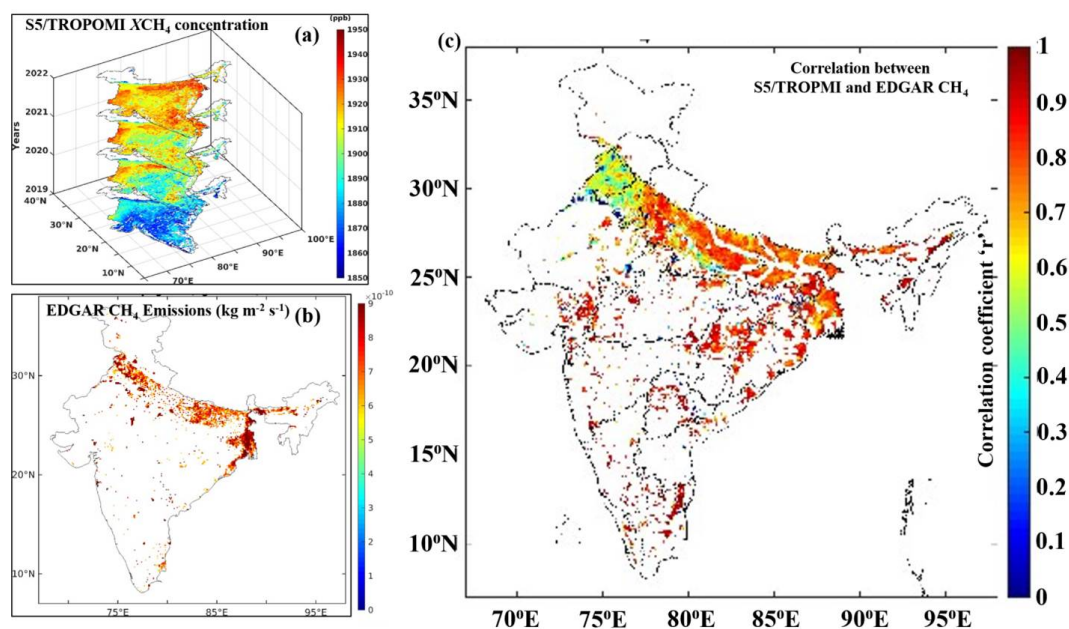
Figure 12. Pixel level correlation between S5P/TROPOMI based a) XCH$_4$ concentrations, b) anthropogenic CH$_4$ bottom-up emission inventory of EDGAR during 2019 to 2022, and c) correlation map.

5 Conclusions

Since the beginning of the Industrial Revolution, growing human populations have resulted in increased waste production, agriculture, and the use of fossil fuels. Therefore, this study demonstrated the spatiotemporal dynamics of XCH$_4$ in the atmosphere and associated natural (wetlands) and anthropogenic sources (coal fields and thermal power plants) in the Indian region. The present study utilized the remote sensing based XCH$_4$ data from the GOSAT and S5P/TROPOMI from 2009 to 2022. The following are the salient findings of the study.

- The present study demonstrated the continuous XCH$_4$ data from the S5P/TROPOMI and GOSAT to effectively monitor the XCH$_4$ dynamics in space and time.

- Long-term trends of XCH$_4$ show significant annual growth from 2009 to 2022 in CH$_4$ over the Indian subcontinent, with a yearly growth rate of 8.76 ppb which is in line with the global trend.

- Long-term temporal and spatial distribution characteristics and variations of CH$_4$ emissions in India have accelerated in the last decade and globally, a substantial diffusion of CH$_4$ is observed from the northern to southern hemisphere.

- XCH$_4$ levels peak in September-October over coal and thermal power plants but reach their minimum during March-May. The seasonal maxima of wetlands vary from site to site and are related to their size and active phase of methanogens.

- Majority of the wetlands show an annual growth rate in XCH$_4$ is about 9.50 ppb year^{-1}, indicates rich in moist habitats and active methanogens process.

- High XCH$_4$ trend of 9.72$\pm$0.41 ppb year^{-1} from the Mundra UMPP, Gujarat as well as the Paschim Bardhman coal mine (slope of 10.15$\pm$0.55 ppb year^{-1}) indicated elevated and significant emissions from fossil fuel industries as compared to other natural sources.

- The highest CH$_4$ emission estimate was observed during the monsoon season over the Sundarbans wetland, the largest protected wetland in India, with a maximum value of 23.62$\pm$3.66 mg m^{-2} month^{-1}. Among the wetland sites, Wular Lake has a rising methane rate of 0.04 mg m^{-2} month^{-1} with a p-value of 0.01.

- The high levels of CH$_4$ emissions seen in the MGP, TGP, UGP, ECPH, LGP, and EGP agroclimatic zones may be related to the varied farming methods and traditional agricultural output in these regions. Most of these areas revolve around the Rice-Wheat farming system which is negatively impacting the climate.

- The spatial patterns of XCH$_4$ concentrations agree well with the high-emission regions. The correlation coefficient 'r' is strongly agreed in the IGP region.

- Therefore we conclude that the space based XCH$_4$ dataset provides significant support to track long-term changes in CH$_4$ and provides insightful information on the causes and feedback mechanisms for the elevated concentrations of methane across the south Asia region.

References

Ahmad, L., Kanth, R., Parvaze, S., and Mahdi, S.: Agro-climatic and Agro-ecological Zones of India. In: Experimental Agrometeorology: A Practical Manual. Springer, Cham., 99-118, https://doi.org/10.1007/978-3-319-69185-5_15, 2017.

Balcombe, P., Speirs, J. F., Brandon, N. P., and Hawkes, A. D.: Methane emissions: Choosing the right climate metric and time horizon, Environ Sci Process Impacts, 20(10), 1323–1339, https://doi.org/10.1039/C8EM00414E, 2018.

Bassi, N., Dinesh, K. M., Anuradha, S., and PardhaSaradhi, P.: Status of wetlands in India: A review of extent, ecosystem benefits, threats and management strategies, J. Hydrol. Reg. Stud., 2, 1, 2014.

Behera, M. D., Mudi, S., Shome, P., Das, P. K., Kumar, S., Joshi, A., Rathore, A., Deep, A., Kumar, A., Sanwariya, C., and Kumar, N.: COVID-19 slowdown induced improvement in air quality in India: Rapid assessment using Sentinel-5P TROPOMI data, Geocarto International, 37(25), 8127-8147, https://doi.org/10.1080/10106049.2021.1993351, 2022.

Bloom, A. A., Bowman, K. W., Lee, M., Turner, A. J., Schroeder, R., Worden, J. R., Weidner, K. C., McDonald, K. C., and Jacob, D. J.: A global wetland methane emissions and uncertainty dataset for atmospheric chemical transport models (WetCHARTs version 1.0), Geosci. Model Dev., 10, 2141–2156, https://doi.org/10.5194/gmd-10-2141-2017, 2017a.

Bloom, A. A., Bowman, K. W., Lee, M., Turner, A. J., Schroeder, R., Worden, J. R., Weidner, K. C., McDonald, K. C., and Jacob, D. J.: CMS: Global 0.5-deg Wetland Methane Emissions and Uncertainty (WetCHARTs v1.0), ORNL DAAC, Oak Ridge, Tennessee, USA, https://doi.org/10.3334/ORNLDAAC/1502, 2017b.

Bloom, A. A., Bowman, K. W., Lee, M., Turner, A. J., Schroeder, R., Worden, J. R., Weidner, K. C., McDonald, K. C., and Jacob, D. J.: CMS: Global 0.5-deg Wetland Methane Emissions and Uncertainty (WetCHARTs v1.3.1), ORNL DAAC, Oak Ridge, Tennessee, USA, https://doi.org/10.3334/ORNLDAAC/1915, 2021.

Bussmann, I., Achterberg, E. P., Brix, H., Brüggemann, N., Flöser, G., Schütze, C., and Fischer, P.: Influence of wind strength and direction on diffusive methane fluxes and atmospheric methane concentrations above the North Sea, Biogeosciences, 21(16), 3819-3838, https://doi.org/10.5194/egusphere-2023-3018, 2024.

Chandra, N., Hayashida, S., Saeki, T., and Patra, P. K.: What controls the seasonal cycle of columnar methane observed by GOSAT over different regions in India?, Atmospheric Chemistry and Physics, 17(20), 12633-12643, https://doi.org/10.5194/acp-17-12633-2017, 2017.

Choudhary, B. B., and Sirohi, S.: Understanding vulnerability of agricultural production system to climatic stressors in North Indian Plains: a meso-analysis, Environ. Dev. Sustain., 24, 13522–13541, https://doi.org/10.1007/s10668-021-01997-7, 2022.

Crippa, M., Solazzo, E., Huang, G., Guizzardi, D., Koffi, E., Muntean, M., Schieberle, C., Friedrich, R., and Janssens-Maenhout, G.: High resolution temporal profiles in the Emissions Database for Global Atmospheric Research, Scientific Data, 7(1), p.121, 2020.

Crutzen, P. J., and Zimmermann, P. H.: The changing photochemistry of the troposphere, Tellus B: Chem. Phys. Meteorol., 43(4), 136-151, https://doi.org/10.3402/tellusb.v43i4.15403, 1991.

Feng, L., Palmer, P. I., Zhu, S., Parker, R. J., and Liu, Y.: Tropical methane emissions explain large fraction of recent changes in global atmospheric methane growth rate, Nat. Commun., 13(1), 1378, https://doi.org/10.1038/s41467-022-28989-z, 2022.

Feng, L., Palmer, P. I., Parker, R. J., Lunt, M. F., and Bösch, H.: Methane emissions are predominantly responsible for record-breaking atmospheric methane growth rates in 2020 and 2021, Atmos. Chem. Phys., 23, 4863–4880, https://doi.org/10.5194/acp-23-4863-2023, 2023.

Francis, D., Weston, M., Fonseca, R., Temimi, M., and Alsuwaidi, A.: Trends and variability in methane concentrations over the Southeastern Arabian Peninsula, Front. Environ. Sci., 11, 1177877, https://doi.org/10.3389/fenvs.2023.1177877, 2023.

Frankenberg, C., Aben, I., Bergamaschi, P., Dlugokencky, E. J., Van Hees, R., Houweling, S., Van Der Meer, R., Snel, R., and Tol, P.: Global column-averaged methane mixing ratios from 2003 to 2009 as derived from SCIAMACHY: Trends and variability, J. Geophys. Res. Atmos., 116(D4), https://doi.org/10.1029/2010JD014849, 2011.

Fu, B., Jiang, Y., Chen, G., Lu, M., Lai, Y., Suo, X., and Li, B.: Unraveling the dynamics of atmospheric methane: the impact of anthropogenic and natural emissions, Environ. Res. Lett., 19, 064001, https://doi.org/10.1088/1748-9326/ad4617, 2024.

Ganesan, A. L., Schwietzke, S., Poulter, B., Arnold, T., Lan, X., Rigby, M., Vogel, F. R., van der Werf, G. R., Janssens-Maenhout, G., Boesch, H., Pandey, S., Manning, A. J., Jackson, R. B., Nisbet, E. G., and Manning, M. R.: Advancing scientific understanding of the global methane budget in support of the Paris Agreement, Global Biogeochem. Cy., 33, 1475–1512, https://doi.org/10.1029/2018GB006065, 2019.

Hayashida, S., Ono, A., Yoshizaki, S., Frankenberg, C., Takeuchi, W., and Yan, X.: Methane concentrations over Monsoon Asia as observed by SCIAMACHY: signals of methane emission from rice cultivation, Remote Sens. Environ., 139, 246–256, https://doi.org/10.1016/j.rse.2013.08.008, 2013.

Huang, L., Tang, M., Fan, M., and Cheng, H.: Density functional theory study on the reaction between hematite and methane during chemical looping process, Appl. Energy, 159, 132-144, https://doi.org/10.1016/j.apenergy.2015.08.011, 2015.

IPCC: Climate change: The physical science basis, Contribution of Working Group I to the sixth assessment report of the intergovernmental panel on climate change, 2021.

Kang, M., Mauzerall, D. L., Ma, Z., and Celia, M. A.: Reducing methane emissions from abandoned oil and gas wells: Strategies and costs, Energy Policy, 132, 594-601, https://doi.org/10.1016/j.enpol.2019.05.045, 2019.

Kavitha, M., and Nair, P. R.: Region-dependent seasonal pattern of methane over Indian region as observed by SCIAMACHY, Atmos. Environ., 131, 316-325, https://doi.org/10.1016/j.atmosenv.2016.02.008, 2016.

Kavitha, M., Nair, P. R., Girach, I. A., Aneesh, S., Sijikumar, S., and Renju, R.: Diurnal and seasonal variations in surface methane at a tropical coastal station: Role of mesoscale meteorology, Sci. Total Environ., 631, 1472-1485, https://doi.org/10.1016/j.scitotenv.2018.03.123, 2018.

Kirschke, S., Bousquet, P., Ciais, P., Saunois, M., Canadell, J. G., Dlugokencky, E. J., Bergamaschi, P., Bergmann, D., Blake, D. R., Bruhwiler, L., Cameron-Smith, P., Castaldi, S., Chevallier, F., Feng, L., Fraser, A., Heimann, M., Hodson, E. L., Houweling, S., Josse, B., Fraser, P. J., Krummel, P. B., Lamarque, J.-F., Langenfelds, R. L., Le Quéré, C., Naik, V., O'Doherty, S., Palmer, P. I., Pison, I., Plummer, D., Poulter, B., Prinn, R. G., Rigby, M., Ringeval, B., Santini, M., Schmidt, M., Shindell, D. T., Simpson, I. J., Spahni, R., Steele, L. P., Strode, S. A., Sudo, K., Szopa, S., van der Werf, G. R., Weiss, R. F., Williams, J. E., and Zeng, G.: Three decades of global methane sources and sinks, Nat. Geosci., 6, 813–823, https://doi.org/10.1038/ngeo1955, 2013.

Kozicka, K., Orazalina, Z., Gozdowski, D., and Wójcik-Gront, E.: Evaluation of temporal changes in methane content in the atmosphere for areas with a very high rice concentration based on Sentinel-5P data, Remote Sens. Appl.: Soc. Environ., 30, 100972, https://doi.org/10.1016/j.rsase.2023.100972, 2023.

Kuze, A., Suto, H., Nakajima, M., and Hamazaki, T.: Thermal and near infrared sensor for carbon observation Fourier-transform spectrometer on the Greenhouse Gases Observing Satellite for greenhouse gases monitoring, Appl. Opt., 48(35), 6716-6733, https://doi.org/10.1364/AO.48.006716, 2009.

Lan, X., Thoning, K. W., and Dlugokencky, E. J.: Trends in globally-averaged CH_4, N2O, and SF6 determined from NOAA Global Monitoring Laboratory measurements, Version 2024-01, https://doi.org/10.15138/P8XG-AA10.

405 Lorente, A., Borsdorff, T., Butz, A., Hasekamp, O., Aan De Brugh, J., Schneider, A., Wu, L., Hase, F., Kivi, R., Wunch, D., Pollard, D. F., Shiomi, K., Deutscher, N. M., Velazco, V. A., Parker, R. J., and Jacob, D. J.: Methane emissions are predominantly responsible for record-breaking atmospheric methane growth rates in 2020 and 2021, Atmos. Chem. Phys., 23, 4863–4880, https://doi.org/10.5194/acp-23-4863-2023, 2021.

Lu, X., Jacob, D. J., Zhang, Y., Shen, L., Sulprizio, M. P., Maasakkers, J. D., Varon, D. J., Qu, Z., Chen, Z., Hmiel, B., and Parker, R. J.:
410 Observation-derived 2010-2019 trends in methane emissions and intensities from US oil and gas fields tied to activity metrics, Proc. Natl. Acad. Sci. USA, 120(17), e2217900120, https://doi.org/10.1073/pnas.1814297116, 2023.

Maasakkers, J. D., McDuffie, E. E., Sulprizio, M. P., Chen, C., Schultz, M., Brunelle, L., Thrush, R., Steller, J., Sherry, C., Jacob, D. J., Jeong, S., Irving, B., and Weitz, M.: A gridded inventory of annual 2012–2018 US anthropogenic methane emissions, Environ. Sci. Technol., 57(43), 16276-16288, 2023.

415 Nair, P. R., and Kavitha, M.: Stratospheric distribution of methane over a tropical region as observed by MIPAS on board ENVISAT, Int. J. Remote Sens., 41(21), 8380-8405, 2020.

Pai, S., and Zeriffi, H.: A novel dataset for analysing sub-national socioeconomic developments in the Indian coal industry, IOP SciNotes, 2(1), 014001, https://doi.org/10.1088/2633-1357/abdbbb, 2021.

Parker, R. J., Boesch, H., McNorton, J., Comyn-Platt, E., Gloor, M., Wilson, C., Chipperfield, M. P., Hayman, G. D., and Bloom, A. A.:
420 Evaluating year-to-year anomalies in tropical wetland methane emissions using satellite CH_4 observations, Remote Sens. Environ., 211, 261-275, https://doi.org/10.1016/j.rse.2018.02.011, 2018.

Pathakoti, M., Santhoshi, T., Aarathi, M., Mahalakshmi, D. V., Kanchana, A. L., Srinivasulu, J., Soni, V. K., and Raja, P.: Assessment of spatio-temporal climatological trends of ozone over the Indian region using machine learning, Spat. Stat., 43, 100513, https://doi.org/10.1016/j.spasta.2021.100513, 2021.

425 Peng, S., Lin, X., Thompson, R. L., Xi, Y., Liu, G., Hauglustaine, D., Lan, X., Poulter, B., Ramonet, M., Saunois, M., and Yin, Y.: Wetland emission and atmospheric sink changes explain methane growth in 2020, Nature, 612(7940), 477-482, https://doi.org/10.1038/s41586-022-05588-1, 2022.

Ricaud, P., Sič, B., El Amraoui, L., Attié, J. L., Zbinden, R., Huszar, P., Szopa, S., Parmentier, J., Jaidan, N., Michou, M., and Abida, R.: Impact of the Asian monsoon anticyclone on the variability of mid-to-upper tropospheric methane above the Mediterranean Basin, Atmos.
430 Chem. Phys., 14(20), 11427-11446, https://doi.org/10.5194/acp-14-11427-2014, 2014.

Rocher-Ros, G., Stanley, E. H., Loken, L. C., Casson, N. J., Raymond, P. A., Liu, S., Amatulli, G., and Sponseller, R. A.: Global methane emissions from rivers and streams, Nature, 621(7979), 530-535, https://doi.org/10.1038/s41586-023-06344-6, 2023.

Salimi, S., Almuktar, S. A., and Scholz, M.: Impact of climate change on wetland ecosystems: A critical review of experimental wetlands, J. Environ. Manage., https://doi.org/10.1016/j.jenvman.2021.112160, 2021.

435 Sagar, V. K., Pathakoti, M., Mahalakshmi, D. V., Rajan, K. S., MVR, S. S., Hase, F., and Sha, M. K.: Ground-Based Remote Sensing of Total Columnar CO_2, CH_4, and CO Using EM27/SUN FTIR Spectrometer at a Suburban Location (Shadnagar) in India and Validation of Sentinel-5P/TROPOMI, IEEE Geoscience and Remote Sensing Letters, 19, 1-5, https://doi.org/10.1109/LGRS.2022.3171216, 2022.

Sakalli, A., Cescatti, A., Dosio, A., and Gücel, M. U.: Impacts of 2°C global warming on primary production and soil carbon storage capacity at pan-European level, Climate Services, 7, 64-77, https://doi.org/10.1016/j.cliser.2017.06.002, 2017.

440 Saunois, M., Bousquet, P., Poulter, B., Peregon, A., Ciais, P., Canadell, J. G., Dlugokencky, E. J., Etiope, G., Bastviken, D., Houweling, S., Janssens-Maenhout, G., Tubiello, F. N., Castaldi, S., Jackson, R. B., Alexe, M., Arora, V. K., Beerling, D. J., Bergamaschi, P., Blake, D. R., Brailsford, G., Brovkin, V., Bruhwiler, L., Crevoisier, C., Crill, P., Covey, K., Curry, C., Frankenberg, C., Gedney, N., Höglund-

Isaksson, L., Ishizawa, M., Joos, F., Kim, H.-S., Kleinen, T., Krummel, P., Lamarque, J.-F., Langenfelds, R., Locatelli, R., Machida, T., Maksyutov, S., McDonald, K. C., Marshall, J., Melton, J. R., Morino, I., Naik, V., O'Doherty, S., Parmentier, F.-J. W., Patra, P. K., Peng, C., Peters, G. P., Pison, I., Prigent, C., Prinn, R., Ramonet, M., Riley, W. J., Saito, M., Santini, M., Schroeder, R., Simpson, I. J., Spahni, R., Steele, P., Takizawa, A., Thornton, B. F., Tian, H., Tohjima, Y., Viovy, N., Voulgarakis, A., van Weele, M., van der Werf, G. R., Weiss, R., Wiedinmyer, C., Wilton, D. J., Wiltshire, A., Worthy, D., Wunch, D., Xu, X., Yoshida, Y., Zhang, B., Zhang, Z., and Zhu, Q.: The global methane budget 2000–2012, Earth Syst. Sci. Data, 8, 697–751, https://doi.org/10.5194/essd-8-697-2016, 2016.

Saunois, M., Martinez, A., Poulter, B., Zhang, Z., Raymond, P., Regnier, P., Canadell, J. G., Jackson, R. B., Patra, P. K., Bousquet, P., Ciais, P., Dlugokencky, E. J., Lan, X., Allen, G. H., Bastviken, D., Beerling, D. J., Belikov, D. A., Blake, D. R., Castaldi, S., Crippa, M., Deemer, B. R., Dennison, F., Etiope, G., Gedney, N., Höglund-Isaksson, L., Holgerson, M. A., Hopcroft, P. O., Hugelius, G., Ito, A., Jain, A. K., Janardanan, R., Johnson, M. S., Kleinen, T., Krummel, P., Lauerwald, R., Li, T., Liu, X., McDonald, K. C., Melton, J. R., Mühle, J., Müller, J., Murguia-Flores, F., Niwa, Y., Noce, S., Pan, S., Parker, R. J., Peng, C., Ramonet, M., Riley, W. J., Rocher-Ros, G., Rosentreter, J. A., Sasakawa, M., Segers, A., Smith, S. J., Stanley, E. H., Thanwerdas, J., Tian, H., Tsuruta, A., Tubiello, F. N., Weber, T. S., van der Werf, G. R., Worthy, D. E., Xi, Y., Yoshida, Y., Zhang, W., Zheng, B., Zhu, Q., and Zhuang, Q.: Global Methane Budget 2000–2020, Earth Syst. Sci. Data Discuss., https://doi.org/10.5194/essd-2024-115, in review, 2024.

Schaefer, H., Fletcher, S. E. M., Veidt, C., Lassey, K. R., Brailsford, G. W., Bromley, T. M., Dlugokencky, E. J., Michel, S. E., Miller, J. B., Levin, I., Lowe, D. C., Martin, R. J., Vaughn, B. H., and White, J. W. C.: A 21st century shift from fossil-fuel to biogenic methane emissions indicated by 13CH4, Science, 352, 80–84, https://doi.org/10.1126/science.aad2705, 2016.

Schneising, O., Buchwitz, M., Burrows, J. P., Bovensmann, H., Bergamaschi, P., and Peters, W.: Three years of greenhouse gas column-averaged dry air mole fractions retrieved from satellite – Part 2: Methane, Atmos. Chem. Phys., 9, 443–465, https://doi.org/10.5194/acp-9-443-2009, 2009.

Shaw, J. T., Allen, G., Barker, P., Pitt, J. R., Pasternak, D., Bauguitte, S. J. B., Lee, J., Bower, K. N., Daly, M. C., Lunt, M. F., Ganesan, A. L., Vaughan, A. R., Chibesankunda, F., Lambakasa, M., Fisher, R. E., France, J. L., Lowry, D., Palmer, P. I., Metzger, S., Parker, R. J., Gedney, N., Bareson, P., Cain, M., Lorente, A., Borsdorff, T., and Nisbet, E. G.: Large Methane Emission Fluxes Observed from Tropical Wetlands in Zambia, Global Biogeochem. Cycles, 36(12), e2021GB007261, https://doi.org/10.1029/2021GB007261, 2022.

Song, H., Sheng, M., Lei, L., Guo, K., Zhang, S., and Ji, Z.: Spatial and Temporal Variations of Atmospheric CH$_4$ in Monsoon Asia Detected by Satellite Observations of GOSAT and TROPOMI, Remote Sensing, 15(13), 3389, https://doi.org/10.3390/rs15133389, 2023.

Sreenivas, G., Mahesh, P., Subin, J., Kanchana, A. L., Rao, P. V. N., and Dadhwal, V. K.: Influence of meteorology and interrelationship with greenhouse gases (CO$_2$ and CH$_4$) at a suburban site of India, Atmos. Chem. Phys., 16, 3953-3967, https://doi.org/10.5194/acp-16-3953-2016, 2016.

Sreenivas, G., Mahesh, P., Mahalakshmi, D. V., Kanchana, A. L., Naveen Chandra, Prabir, K., Patra, Raja, P., Shesha Sai, M. V. R., Sripada, S., Rao, P. V., and Dadhwal, V. K.: Seasonal and annual variations of CO$_2$ and CH$_4$ at Shadnagar, a semi-urban site, Sci. Total Environ., 819, 153114, https://doi.org/10.1016/j.scitotenv.2022.153114, 2022.

Taneja, G., Pal, B. D., Joshi, P. K., Aggarwal, P. K., and Tyagi, N. K.: Farmers' preferences for climate-smart agriculture—an assessment in the Indo-Gangetic Plain, Springer, Singapore, 91-111, 2019.

Turner, A. J., Frankenberg, C., and Kort, E. A.: Interpreting contemporary trends in atmospheric methane, Proc. Natl. Acad. Sci. USA, 116, 2805–2813, https://doi.org/10.1073/pnas.1814297116, 2019.

Vinna, L., Medhaug, I., and Schmid, M.: The vulnerability of lakes to climate change along an altitudinal gradient, Commun. Earth Environ., 2, 35, https://doi.org/10.1038/s43247-021-00106-w, 2021.

Wang, Y., Yang, H., Ye, C., Chen, X., Xie, B., Huang, C., Zhang, J., and Xu, M.: Effects of plant species on soil microbial processes and CH_4 emission from constructed wetlands, Environ. Pollut., 174, 273-278, https://doi.org/10.1016/j.envpol.2012.11.020, 2013.

Wei, Y., Yang, X., Qiu, X., Wei, H., and Tang, C.: Spatio-temporal variations of atmospheric methane and its response to climate on the Tibetan Plateau from 2010 to 2022, Atmos. Environ., 120088, https://doi.org/10.1016/j.atmosenv.2023.120088, 2023.

485   Worden, J. R., Bloom, A. A., Pandey, S., Jiang, Z., Worden, H. M., Walker, T. W., Houweling, S., and Röckmann, T.: Reduced biomass burning emissions reconcile conflicting estimates of the post-2006 atmospheric methane budget, Nat. Commun., 8, 1–11, https://doi.org/10.1038/s41467-017-02246-0, 2017.

Zhang, L., Tian, H., Shi, H., Pan, S., Chang, J., Dangal, S. R., and Jackson, R. B.: A 130-year global inventory of methane emissions from livestock: Trends, patterns, and drivers, Global Change Biol., 28(17), 5142-5158, https://doi.org/10.1111/gcb.16280, 2022.

490   Zhang, Z., Poulter, B., Feldman, A. F., Ying, Q., Ciais, P., Peng, S., and Li, X.: Recent intensification of wetland methane feedback, Nat. Clim. Change, 13(5), 430-433, https://doi.org/10.1038/s41558-023-01629-0, 2023.